The role played by different TiO_2 features on the photocatalytic degradation of paracetamol

Luca Rimoldi [a,b,*], Daniela Meroni[a,b,*], Ermelinda Falletta [a], Anna Maria Ferretti [c], Antonella Gervasini[a], Giuseppe Cappelletti[a,b], Silvia Ardizzone[a,b]

[a] *Dipartimento di Chimica, Università degli Studi di Milano, Via Golgi 19, 20133 Milano, Italy*

[b] *Consorzio Interuniversitario Nazionale per la Scienza e la Tecnologia dei Materiali (INSTM), Via Giusti 9, 50121 Firenze, Italy*

[c] *ISTM-CNR Lab Nanotechnology, Via Fantoli 16/15 Milano, Italy*

[*] *Corresponding authors: luca.rimoldi@unimi.it; daniela.meroni@unimi.it*

ABSTRACT

Photocatalytic reactions promoted by TiO_2 can be affected by a large number of oxide features (*e.g.* surface area, morphology and phase composition). In this context, the role played by the surface characteristics (*e.g.* surface acidity, wettability, *etc.*) has been often disregarded. In this work, pristine and Ta-doped TiO_2 nanomaterials with different phase composition (pure anatase and anatase/brookite mixture) were synthesized by sol-gel and characterized under the structural and morphological point of view. A careful characterization of the acid properties of the materials has been performed by liquid-solid acid-base titration by means of 2-phenylethylamine (PEA) adsorption to determine the acid site density and average acid strength. Photocatalytic tests were performed in the degradation of paracetamol (acetaminophen) under UV irradiation and results were discussed in the light of the detailed scenarios describing the different oxides. The surface acidity of the samples, was recognized as one of the key parameters controlling the photocatalytic activity. A possible molecule degradation route is proposed on the ground of GC-MS and ESI-MS analyses.

KEYWORDS

Titanium dioxide photocatalysis, Ta-doped TiO_2, surface acidity, phenylethylamine, acetaminophen degradation, HR-TEM

1. INTRODUCTION

Titanium dioxide (TiO_2) finds applications in several fields of material science and nanotechnology [1,2]. Modification and/or functionalization of its surface is a widely adopted technique for the preparation of manifold hybrid materials, inorganic-organic devices, promoted photocatalysts [3–6].

Different modifications of TiO_2 can strongly affect the properties of this material. This is especially so in the case of TiO_2 applications in photocatalysis where both bulk and surface oxide features can differently, or even divergently, affect the final performance of the reaction. The choice of the synthetic route to obtain the oxide is often crucial in this respect.

The temperature of the oxide preparation, for instance, is one of the key parameters to be controlled or modulated in the synthesis of a photocatalyst [7]. In fact, on one side, high temperature promotes crystallinity and surface regularity reducing recombination between charge carriers; at the same time, however, the growth of the crystallites and their aggregation may support loss of surface area and porosity, lowering the active photocatalyst surface.

Recently the use of metal species was proposed to promote TiO_2 efficiency in photocatalytic applications [8–10]. The introduction of metal species may relevantly modify the structural, electronic, optical and morphological properties of the material. Besides metals of the first transition series, the doping by niobium and tantalum was recently suggested, on the grounds of both theoretical and experimental results, to promote the oxide photocatalytic activity, due to the electronic configuration of their 4 and 5 d orbitals [11]. In the case of Nb/N codoped materials, the choice of the procedure adopted to dope the oxide by the guest species appeared to be decisive: the sample obtained by including the dopants during the oxide synthesis showed the best performance under solar irradiation while the sample obtained by impregnation appeared to be the slowest photocatalyst even with respect to undoped TiO_2 [12,13].

Apart from modifications of the bulk and electronic features of a material, the surface acidity of a photocatalyst can be expected to appreciably affect the course of the reaction. These aspects are not extensively debated in the literature and several apparent diverging results can be found. Both enhancement [14–16] and decreasing [17–20] of the photocatalytic performance due to a stronger surface acidity were reported in the case of TiO_2 materials. Yamazaki *et al.* also described a decrease of activity of the photocatalyst due to the transformation of Lewis sites to Broensted, during the reaction [21].

In the present work, we synthesized and characterized two pristine TiO_2 nanostructured samples showing different phase composition and the two relative Ta-doped samples obtained by impregnation. Further, a comparative analysis of the intrinsic surface acidity of the nanomaterials by acid-base titration with adsorption of 2-phenylethylamine (PEA) probe was performed [22,23]. The results of the different characterizations are discussed in the light of the samples photocatalytic performance in the oxidative degradation of paracetamol. The choice of the target molecule is to be considered in the context of emerging contaminants pollution of surface, ground and wastewaters, which attracted much attention in the scientific community in the last few years [24–26].

2. MATERIALS AND METHODS

All products were purchased by Sigma-Aldrich and used without any further purification. Solutions and suspensions were prepared adopting doubly-distilled water passing through a Milli-Q apparatus.

2.1 Materials synthesis

The nanostructured powders were prepared by two different sol-gel procedures.

The first procedure was previously reported elsewhere [12]. In brief, in a three-necked flask, isopropanol and Ti(IV)isopropoxide were mixed and then the Ti precursor was hydrolyzed by dropping a HCl aqueous solution at pH = 3 in 30 min under vigorous stirring. The sol was kept under stirring for 1 h and successively put in an oven at 90 °C to dry. The recovered powder was finally calcined at 400 °C for 6 h under O_2 flux (9 NL h^{-1}). The sample was labelled T. An impregnation method in a $TaCl_5$ water-ethanol solution was adopted before the calcination step to obtain the corresponding Ta-doped sample, with a molar ratio Ti/Ta = 1 %. The Ta-doped sample was labelled TTa.

The second procedure [7] implied the formation of a Ti(IV)isopropoxide and acetic acid mixture in a three-necked flask and a successive drop-by-drop hydrolysis with water under vigorous stirring, for 30 min at 0 °C. The sol was kept under stirring for 1 h and later put in an oven at 70 °C for 3 h and then at 100 °C to dry. Finally, the amorphous powder was calcined at 400 °C for 6 h under O_2 flux (9 NL h^{-1}). The sample was labelled TAC. The same impregnation procedure described above was adopted to obtain the sample doped with Ta. The Ta-doped sample was named TTaAC.

2.2 Materials Characterization

X-Ray Powder Diffraction (XRPD). The nanomaterials were characterized by XRPD experiments. A Philips PW 3710 Bragg-Brentano goniometer instrument equipped with a scintillation counter and 1° divergence slit, 0.2 mm receiving slit, and 0.04° Soller slit systems was adopted. Graphite-monochromated Cu Kα radiation at 40 kV × 40 mA nominal X-ray power was employed. θ:2θ scans were performed between 20° and 90°. The phase composition was determined by a least-square approach to refine the theoretical line profile until it matches the measured XRD pattern. In the present work, the Quanto software, developed by C. Giacovazzo, A. Gagliardi *et al.* at the University of Bari, based on the Rietveld refinement, was adopted. Background was modelled using a Young polynomial, while experimental points were interpolated using a Pearson VII function. 2θ−zero shift background coefficients, cell constants, scale factor, FWHM and other terms were refined using a least squares approach.[7]. The average crystallite size of the anatase phase was estimated applying the Scherrer equation on the (101) peak.

High resolution transmission electron microscopy (HR-TEM). The transmission electron analyses were performed using Zeiss Libra FE 200 keV, equipped with in column second generation Omega filter for energy selected spectroscopy. The TEM samples were prepared following this procedure: first the nanostructured powders were finely smashed in a mortar, then suspended in isopropanol and finally sonicated 15 minutes. Immediately after sonication process the suspensions were dropped onto a holey carbon coated copper TEM grid. All specimens were dried at room temperature for 24 h. The micrograph analyses were performed using the iTEM (TEM Imaging) Platform software (Olympus). The equivalent diameter was estimated calculating the median of the distribution.

Specific Surface Area and Porosity Determinations. A Coulter SA3100 apparatus was used to determine specific surface areas by the Brunauer-Emmett-Teller (BET) method. Before the measurement the samples were outgassed at 150 °C for 2 h under vacuum. Pore size distributions were determined from the desorption isotherms by the Barrett-Joyner-Halenda (BJH) method.

X-ray Photoelectron Spectroscopy (XPS). An M-probe apparatus (Surface Science Instruments) was adopted to perform X-ray Photoelectron Spectroscopy (XPS) analyses, employing a monochromatic Al Kα radiation (1.486 keV) with spot size of 200 μm x 750 μm and pass energy of 25 eV. Internal referencing at C 1s (284.6 eV) was adopted to correct for charge build-up. Ta content was determined by elaboration of Survey spectra.

Surface acidity measurements. Experiments were performed in a modified liquid chromatograph (HPLC), equipped with a UV detector coupled to a personal computer for the collection, storage and processing of the data, especially set-up for realizing acid-base titrations in liquid-solid phase [23]. For each experiment, a weighed amount (*ca*. 0.1 g) of fresh sample was introduced into the sample holder maintained in an oven for 4 h at 150 °C under flowing air, then evacuated and filled with cyclohexane under vacuum. In each adsorption test performed at 25 ± 1 °C, pulses (50 μL) of 2-phenyethylamine (PEA) solution in cyclohexane of known concentration were sent at fixed time intervals (10 min) onto the sample at a constant solvent flow rate (5 mL min^{-1}). The non-adsorbed amounts of PEA after each pulse were detected up to sample saturation, corresponding to the obtainment of chromatographic peaks of equal area.

The amount of amine adsorbed on the catalyst sample after the i-th pulse was calculated via the following equation:

$$(\text{amine adsorbed})_i\ [\text{meq g}^{-1}] = (V \cdot C/w)\ (A_{av} - A_i)\ A_{av} \quad (1)$$

where V (mL) corresponds to the volume a single pulse, C (mol L^{-1}) is the concentration of the amine solution, w (g) is the mass of the sample, A_{av} is the mean chromatographic area at saturation and A_i is the area corresponding to the i-th pulse.

If a 1:1 adsorption stoichiometry is assumed, the total number of acidic sites corresponds to the total amount of amine adsorbed on the sample surface.

$$\text{acidic sites}\ [\text{meq g}^{-1}] = \Sigma_i\ (\text{amine adsorbed})_i\ [\text{meq g}^{-1}] \quad (2)$$

After the 1st run adsorption on the fresh sample, a 2nd run was performed after elution of pure solvent for 30 min, to determine the strong acidity of the samples by subtracting the acid sites titrated in the 2nd run (weak acid sites) from those of the 1st run adsorption (total acid sites).

Suspension stability tests. The different samples were suspended in water (about 7 g L^{-1}) and sonicated for 15 min. Successively the absorbance of the suspension at 500 nm was recorded by a Shimadzu UV-2600 UV-vis spectrophotometer as a function of time.

2.3 Photocatalytic tests

All samples were tested in the photocatalytic degradation of paracetamol in ultrapure water, under UV irradiation, adopting a Jelosil HG500 lamp (30 mW cm^{-2}). A 600 mL jacketed reactor termostated at 20 °C was used. An initial paracetamol concentration of 35 mg L^{-1} and a catalyst amount of 0.5 g L^{-1} were selected. An O_2 flux was bubbled in the reactor during the reaction (9 NL h^{-1}). The molecule degradation was followed by UV-vis spectroscopy by detecting the decreasing intensity of the typical absorption peak of paracetamol at 243 nm with respect to time, while Total Organic Carbon (TOC) measurements allowed the mineralization degree to be calculated. The reaction was followed for 2 h.

Gas Chromatography-Mass Spectroscopy (GC-MS) and Electronspray Ionization Mass Spectroscopy (ESI-MS) analyses. In order to identify reaction intermediates of paracetamol photocatalytic degradation, both GC-MS and ESI-MS measurements were performed by using an ISQ™ QD Single Quadrupole GC-MS (Thermo Fisher) and a Thermo Finnigan (MA, USA) LCQ Advantage system MS spectrometer with an electrospray ionization source and an 'Ion Trap' mass analyser. Regarding GC-MS, the injection temperature was fixed at 250 °C with a flow of 1.2 mL min^{-1} and a ZB-1MS 60 m (0.25 μm I.D.; 0.25 μm thickness) column, fixing at 260 °C the transfer line temperature and at 250 °C the ion source temperature. ESI-MS analyses were performed by solubilizing the samples in methanol. Formic acid was added in order to enhance the sample volatility. MS spectra were obtained by direct infusion of the sample solutions under ionization, ESI positive by applying +3.0 kV at the entrance of the capillary with the drying gas heated to 350 °C. Full-scan mass spectra were recorded in the mass/charge (m/z) range of 50 – 1000.

3. RESULTS

3.1 Characterization results

For all samples the phase composition was assessed by Rietveld refinement by adopting the Quanto software [7]. XRPD analyses revealed the predominant polymorph to be anatase for all synthesized samples (Fig. 1). The series of samples prepared by hydrolysis with HCl solution (T and TTa) contained both anatase and brookite (*ca.* 60% anatase and 40% brookite), with small variations between the Ta-doped and the undoped samples (Tab. 1). In Fig. 1 the most intense peak of the anatase phase, (101), was labelled (θ = 25°). In the case of brookite, the (121) peak was marked since it is the only isolated peak of this phase, not overlapping with the anatase lines (θ = 31°). Differently, the nanostructured materials synthesized in the presence of acetic acid (TAC and TTaAC) are mainly composed by anatase, due to the action of acetic acid as promoting species, as reported elsewhere [27]. In both cases, the presence of Ta did not seem to modify the phase composition of the samples. Conversely, the effect of the guest species is clear on the average crystallite dimensions, calculated by applying the Scherrer equation to (101) anatase reflections: while pristine samples had a crystallite diameter of *ca.* 7 nm, Ta-doped nanomaterials reached slightly bigger dimensions (*ca.* 9 nm) (Tab. 1; Fig. S1). TEM images allowed to recognize a certain aggregation among the crystallites, found to be comparable for all samples (Fig. 2; Figs. S2-S4). HR-TEM analyses confirmed the information retrieved by XRPD about the crystallites dimension and the trend upon impregnation treatment (Tab. 1). We reported both the average and the mode of the equivalent crystallites diameter, because the mode represents the more probable value and it is more representative of the morphology of the nanocrystals. Anyway, it is not worthless to consider also the mean size because this parameter was fully comparable with the results obtained by the Scherrer equation (Tab. 1). The phase composition of the different samples previously obtained by XRPD analyses, was confirmed also by the electron diffraction (ED) powder pattern (Fig. S5). Both anatase and brookite monocrystals were identified for the T and TTa biphasic samples, by applying Fast Fourier Transform, clearly exhibiting the typical patterns of the two titania polymorphs (Fig. 2).

N_2 adsorption-desorption isotherms of all samples present the typical profile of mesoporous materials, classified as IV-type according to the IUPAC classification (Fig. 3a). The B.E.T. calculation revealed higher specific surface area for the TAC sample (173 m^2 g^{-1}), with respect to

the corresponding mixed phase powder, T (153 m^2 g^{-1}). In both cases, the doping procedures affect the surface area parameter by a decrease of *ca.* 40 m^2 g^{-1} (Tab. 1), in agreement with the increase of the crystallite sizes observed by XRD and with particle aggregation shown by TEM images. Regarding hysteresis loop shapes, TAC exhibited a strong H2-type shape, characteristic of bottle-neck shaped pores. This profile is less marked for T, even if characterized by H2 hysteresis loop, in its turn (Fig. 3a). Under this point of view, no significant difference was found upon Ta-doping. The position of the hysteresis loop revealed TAC sample to have smaller pores with respect to T. Moreover, the total porosity of the samples is observed to decrease appreciably upon Ta impregnation in the case of the mixed phase T sample (Fig. 3b).

In the case of the Ta-impregnated samples the amount of Ta was analysed by XPS. These analyses appear to be affected by a large noise, possibly due to the low amount of the added Ta species. Fig. S6 reports the XPS Ta 4f region in the case of TTa. For the doped samples the experimental atomic Ta/Ti ratio was found in the range 0.02-0.06 indicating a surface Ta enrichment due to impregnation procedure.

The surface acidity of the four samples was evaluated by liquid-solid acid-base titration by using PEA as basic probe. All the obtained results are collected in Fig. 4, in which the adsorbed PEA is reported for all samples (1^{st} run adsorption) as a function of the injected PEA. The collected curves have hyperbolic shape with attainment of a *plateau* value for the adsorbed PEA, which corresponds to saturation of all surface acid sites. In particular, the three samples, TAC, TTa, and TTaAC showed high acidity, while T sample did not possess acid surface. As expected, the most acidic samples correspond to those synthesized in the presence of acetic acid (TTaAC and TAC); also, the Ta-doped sample (TTa) showed a well-developed surface acidity. Table 2 reports the results in terms of total acid sites (meq g^{-1}) including the strong acid sites which correspond to 77%, for TTa, 84% for TAC, and 90% for TTaAC, evaluated comparing the 1^{st} and 2^{nd} runs of PEA adsorption. As the samples have different surface area values (Table 1), the acid site density of the samples, calculated for surface unity (μeq m^{-2}), does not follow the same ranking (Table 2, second and third columns). The Ta-doped sample has higher acid site density than TAC with a lower percent of strong acid sites than TAC (Table 2, fourth column).

The suspension stability in water was evaluated by spectrometry. All samples give rise to relatively stable suspensions, the absorbance decreasing at maximum by about 6% after 1 h. The T sample revealed to be the most stable photocatalyst. The Ta-doping procedure resulted in an increased instability in aqueous suspension, the more so for the TTaAC sample (Fig. 5).

3.2 Photocatalytic results

While most of the literature uses dyes as model water pollutants [28,29], the present samples were tested in the photocatalytic degradation of paracetamol under UV irradiation. In a short time-scale (2 h) 70-80% of degradation was achieved, together with high mineralization degrees, between 44 and 59%, depending on the sample (Fig. 6, Tab. 3). T sample revealed to be the most efficient regarding both molecule disappearance and mineralization, although not showing the highest surface area among the different samples. The oxidative photodegradation proceeded more slowly for the other three samples, with small differences concerning the molecule disappearance. Under the mineralization point of view, the TTa sample showed the lowest performance (44%), while the other two samples exhibited similar behaviour in terms of mineralization.

While the molecule disappearance reaches values of 70-80% at the end of the photocatalytic test, TOC data showed that only 40-60% of the organic carbon is fully mineralized in the considered reaction time, suggesting significant presence of reaction intermediates. Figs. S7 and S8 shows the ESI-MS spectra in the positive ion mode of the initial paracetamol solution and after 120 min of irradiation during tests with both T and TAC samples. All spectra exhibit as main features two peaks at m/z = 152 and m/z = 174, which can be attributed to protonated paracetamol $[M + H]^+$ and $[M + Na]^+$, respectively. At the end of the degradation process, the intensity of the paracetamol peaks decreases as expected. Similar results were obtained in ESI-MS spectra in the negative ion mode (data not shown), where the main peak was at m/z = 150 (deprotonated paracetamol, $[M - H]^-$). Upon light irradiation (spectra after 65 min, not shown, and 120 min), the presence of other ions in the mass spectra (m/z = 79, 95, 108 and 130) becomes appreciable; these peaks, which are in good agreement with the literature, may represent reaction intermediates, although their attribution is difficult due to their low concentrations [30]. It is noteworthy that no significant differences in the detected peaks could be observed between the different samples, although their relative concentration varies. GC-MS analyses were also carried out to identify the degradation intermediates of the reaction for the two undoped samples after 0, 65 and 120 min of irradiation. Fig. 7 reports the MS fragmentation profiles of the main identified intermediates which are in good agreement with previous investigations of paracetamol degradation by TiO_2/UV and UV/H_2O_2 [30–33]. The contemporary presence of aminophenol and acetamide suggests the parallel occurrence of competitive reaction pathways involving $^{\bullet}OH$ radicals. In particular, the presence of acetamide suggests an early cleavage of the $–NHCOCH_3$ moiety of the paracetamol molecule, possibly following the attack of hydroxyl radicals at a para position with respect to the –OH group of paracetamol [30,33,34]. The resulting hydroquinone intermediate is known to produce p-benzoquinone by successive $^{\bullet}OH$ oxidation, which is known to be unstable and tends to undergo ring rupture giving rise to open ring dicarboxylic acids [35]. The detection of aminophenol supports instead the alternative degradation mechanism proposed by Moctezuma *et al.* [31], involving a deacylation reaction pathway.

4. DISCUSSION

The synthetic procedure adopted to prepare the present TiO_2 samples is found to markedly affect the final oxide features and, consequently, their photocatalytic activity. The sol-gel T sample obtained in the presence of HCl shows the best activity, although presenting a specific surface area of 20 $m^2\ g^{-1}$ lower than TAC (largest surface area of all samples). The photocatalytic activity is often due to an interplay of different properties [36]. In the present case, morphological properties alone cannot explain the observed activity sequence, as shown by the comparison of the photocatalytic performance of the two undoped samples. The sol-gel T sample obtained in the presence of HCl shows the best activity. Several factors can be invoked to interpret these finding. The oxide is composed by both anatase and brookite and the presence of different polymorphs has often been invoked to reduce recombination due to charge separation effects [37]. Moreover, the T aqueous suspension shows the best stability in time, supporting a fast approach by the pollutant and its intermediates. A relevant role is played by the acidity features of the present samples. The T sample is definitely the sample showing the lowest content of acid sites. The relevant acidity of TAC may be traced back to the large amount of acetic acid adopted to promote the anatase

structure. The selective promotion of a given structural crystalline lattice is the result of strong chemisorption phenomena occurring at given facets [38]. In the case instead of the Ta-promoted samples, the pentavalent guest species promote the formation of Lewis acid Ti^{3+} moieties, thus enhancing the surface acidity. On the grounds of XPS results, the prevailing surface enrichment of Ta species supports an appreciable modification of the surface properties of the metal doped samples. The acidic features, together with the lowest value of the specific surface area, may be invoked to be responsible for the low photocatalytic efficiency of the TTa sample. The role played by the acid features of a photocatalyst is poorly discussed in the literature with controversial results. For example, Kozlov *et al.* reported promotion of acetone photodegradation in the gas phase by increasing the acidity of sulphate-doped TiO_2 [16]. Conversely, in the case of the photodegradation of phenol in the liquid phase, Colón *et al.* showed a decreasing performance by increasing the acidity of sulphated TiO_2 [20]. The degradation of paracetamol may show similarities with that of phenol supporting the agreement between the present results and those by Colón *et al.*. The paracetamol molecule shows a pK_a of 9.38 and therefore at the pH adopted in the present experiment (pH = 5.5) the molecule is neutral and simple electrostatic effects can be excluded. No indications of different reaction routes among the different samples are given by GC-MS and ESI results. Since the increasing acid features affect to a larger extent the final mineralization than the molecule disappearance (Tab. 3), we can suggest that basic intermediates (*p*-aminophenol, acetamide, *etc.*) may remain strongly bound at the photocatalyst acid surface sites, thus blocking the access at the active surface.

On the grounds of the mass characterizations, the parallel reaction pathways reported in Scheme 1 can be proposed, also according to previous reports concerning TiO_2/UV and H_2O_2/UV degradation of paracetamol [31,34].

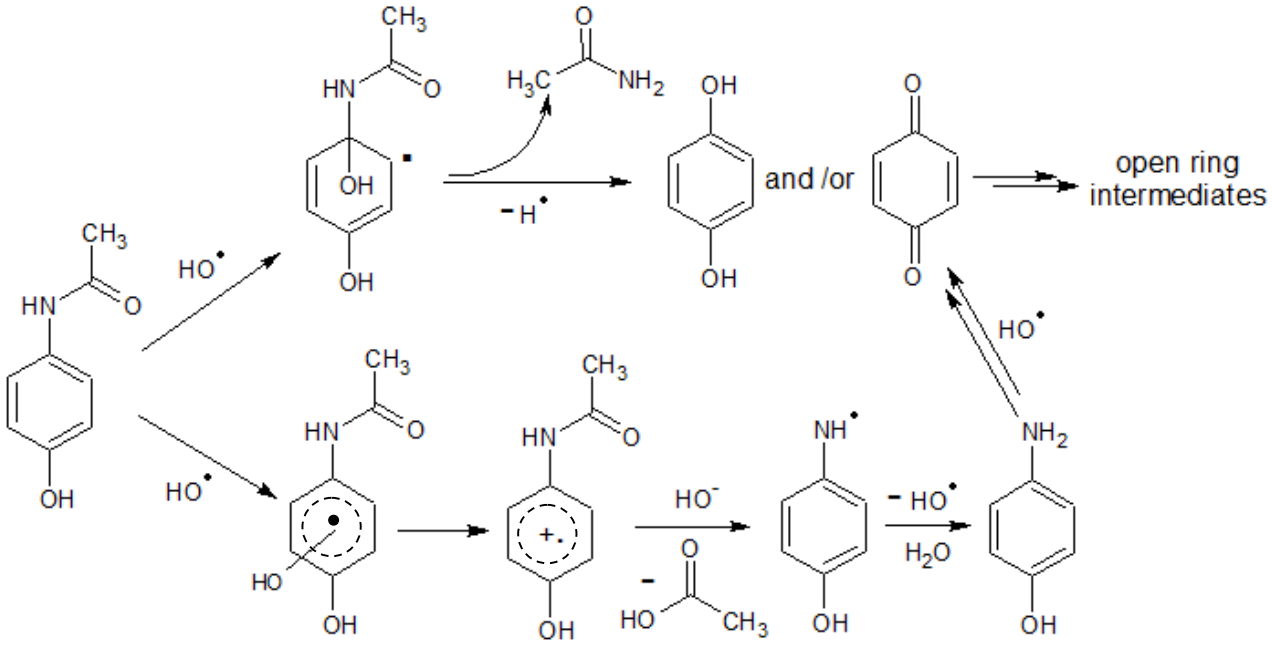

Scheme 1 – Proposed reaction pathways of paracetamol degradation.

This suggested mechanism may allow us to interpret the different role played by Ta-doped TiO_2 on the photocatalytic degradation of different pollutants under UV irradiation. In a previous work, Ta-

promoted samples showed an improved performance with respect to pristine TiO_2 in the gas phase degradation of ethanol, which proceeds by acidic intermediates [12].

5. CONCLUSIONS

Different TiO_2 samples, both pristine and Ta-doped, were obtained in the laboratory by sol-gel procedures combined with mild calcinations. The two pure TiO_2 samples are composed either by an anatase/brookite mixture or by pure anatase. The addition of Ta species by impregnation does not modify the phase composition with respect to the relative pure oxide but it provokes an increase in the crystallite sizes with an ensuing decrease of the specific surface area and an increase of the surface acidity.

All samples give rise to relatively stable suspensions in water the more so in the case of the pristine anatase/ brookite mixture. This latter sample is the one showing the lowest content of acidic groups, while all other samples show markedly acidic features.

The photocatalytic degradation of paracetamol, an emerging pollutant, was studied in aqueous suspensions of the photocatalysts. A balance of different factors can be proposed as the origin of the best performance shown by the anatase/brookite pristine sample:

- highly accessible surface sites (large surface area and pore volume, excellent stability in water);
- the presence of the two TiO_2 polymorphs which can reduce charge carrier recombination effects;
- the very low content of acid sites.

The first two points can be considered to bear a general significance in the case of photocatalytic reactions performed in aqueous media. The effects, instead, introduced by the surface acidity, appear to be more strictly related to the physicochemical pollutant features and, mainly, to its degradation intermediates. In fact, the study of the reaction pathway suggests the occurrence of basic intermediate species which might remain strongly adsorbed at the oxide acid sites, thus reducing the total mineralization of the process.

REFERENCES

[1] A. Fujishima, X. Zhang, D.A. Tryk, TiO_2 photocatalysis and related surface phenomena, Surf. Sci. Rep. 63 (2008) 515–582. doi:10.1016/j.surfrep.2008.10.001.

[2] L. Rimoldi, D. Meroni, E. Falletta, V. Pifferi, L. Falciola, G. Cappelletti, et al., Emerging pollutant mixture mineralization by TiO_2 photocatalysts. The role of the water medium, Photochem. Photobiol. Sci. 16 (2017) 60–66. doi:10.1039/C6PP00214E.

[3] Y. Liang, H. Wang, H. Sanchez Casalongue, Z. Chen, H. Dai, TiO_2 nanocrystals grown on graphene as advanced photocatalytic hybrid materials, Nano Res. 3 (2010) 701–705. doi:10.1007/s12274-010-0033-5.

[4] T. Khoa Le, D. Flahaut, H. Martinez, H.K. Hung Nguyen, T.K. Xuan Huynh, Study of the effects of surface modification by thermal shock method on photocatalytic activity of TiO_2 P25, Appl. Catal. B Environ. 165 (2015) 260–268. doi:10.1016/j.apcatb.2014.10.024.

[5] P. Gorbovyi, A. Uklein, S. Tieng, O. Brinza, M. Traore, K. Chhor, et al., Novel

nanostructured pHEMA–TiO_2 hybrid materials with efficient light-induced charge separation, Nanoscale. 3 (2011) 1807. doi:10.1039/c0nr00909a.

[6] C. Xue, T. Wang, G. Yang, B. Yang, S. Ding, A facile strategy for the synthesis of hierarchical TiO_2/CdS hollow sphere heterostructures with excellent visible light activity, J. Mater. Chem. A. 2 (2014) 7674. doi:10.1039/c4ta01190b.

[7] L. Rimoldi, D. Meroni, G. Cappelletti, S. Ardizzone, Green and low cost tetracycline degradation processes by nanometric and immobilized TiO_2 systems, Catal. Today. 281 (2017) 38–44. doi:10.1016/j.cattod.2016.08.015.

[8] A. Sengele, D. Robert, N. Keller, V. Keller, A. Herissan, C. Colbeau-Justin, Ta-doped TiO_2 as photocatalyst for UV-A activated elimination of chemical warfare agent simulant, J. Catal. 334 (2016) 129–141. doi:10.1016/j.jcat.2015.11.004.

[9] R. Long, N.J. English, Band gap engineering of (N,Ta)-codoped TiO_2: A first-principles calculation, Chem. Phys. Lett. 478 (2009) 175–179. doi:10.1016/j.cplett.2009.07.084.

[10] X. Yan, C. Xue, B. Yang, G. Yang, Novel three-dimensionally ordered macroporous Fe^{3+}-doped TiO_2 photocatalysts for H_2 production and degradation applications, Appl. Surf. Sci. 394 (2017) 248–257. doi:10.1016/j.apsusc.2016.10.077.

[11] L.R. Sheppard, S. Hager, J. Holik, R. Liu, S. Macartney, R. Wuhrer, Tantalum Segregation in Ta-Doped TiO_2 and the Related Impact on Charge Separation during Illumination, J. Phys. Chem. C. 119 (2015) 392–400. doi:10.1021/jp509806h.

[12] L. Rimoldi, C. Ambrosi, G. Di Liberto, L. Lo Presti, M. Ceotto, C. Oliva, et al., Impregnation versus Bulk Synthesis: How the Synthetic Route Affects the Photocatalytic Efficiency of Nb/Ta:N Codoped TiO_2 Nanomaterials, J. Phys. Chem. C. 119 (2015) 24104–24115. doi:10.1021/acs.jpcc.5b06827.

[13] C. Marchiori, G. Di Liberto, G. Soliveri, L. Loconte, L. Lo Presti, D. Meroni, et al., Unraveling the Cooperative Mechanism of Visible-Light Absorption in Bulk N,Nb Codoped TiO_2 Powders of Nanomaterials, J. Phys. Chem. C. 118 (2014) 24152–24164. doi:10.1021/jp507143z.

[14] K.K. Akurati, A. Vital, J. Dellemann, K. Michalow, T. Graule, D. Ferri, et al., Flame-made WO_3/TiO_2 nanoparticles: Relation between surface acidity, structure and photocatalytic activity, Appl. Catal. B Environ. 79 (2008) 53–62. doi:10.1016/j.apcatb.2007.09.036.

[15] J. Papp, S. Soled, K. Dwight, A. Wold, Surface Acidify and Photocatalytic Activity of TiO_2, WO_3/TiO_2, and MoO_3/TiO_2 Photocatalysts, Chem. Mater. (1994) 496–500.

[16] D. Kozlov, D. Bavykin, E. Savinov, Effect of the acidity of TiO_2 surface on its photocatalytic activity in acetone gas-phase oxidation, Catal. Letters. 86 (2003) 169–172. doi:10.1023/A:1022651615366.

[17] J. Yu, J.C. Yu, M.K.-P. Leung, W. Ho, B. Cheng, X. Zhao, et al., Effects of acidic and basic hydrolysis catalysts on the photocatalytic activity and microstructures of bimodal mesoporous titania, J. Catal. 217 (2003) 69–78. doi:10.1016/S0021-9517(03)00034-4.

[18] M.D. Hernández-Alonso, A.R. Almeida, J.A. Moulijn, G. Mul, Identification of the role of surface acidity in the deactivation of TiO_2 in the selective photo-oxidation of cyclohexane, Catal. Today. 143 (2009) 326–333. doi:10.1016/j.cattod.2008.09.025.

[19] L. Zhang, V.M. Menendez-Flores, N. Murakami, T. Ohno, Improvement of photocatalytic activity of brookite titanium dioxide nanorods by surface modification using chemical

etching, Appl. Surf. Sci. 258 (2012) 5803–5809. doi:10.1016/j.apsusc.2012.02.103.

[20] G. Colón, M.C. Hidalgo, J.A. Navío, A. Kubacka, M. Fernández-García, Influence of sulfur on the structural, surface properties and photocatalytic activity of sulfated TiO_2, Appl. Catal. B Environ. 90 (2009) 633–641. doi:10.1016/j.apcatb.2009.04.026.

[21] S. Yamazaki, K. Ichikawa, A. Saeki, T. Tanimura, K. Adachi, Photocatalytic Degradation of Chlorinated Ethanes in the Gas Phase on the Porous TiO_2 Pellets: Effect of Surface Acidity, J. Phys. Chem. A. 114 (2010) 5092–5098. doi:10.1021/jp911842t.

[22] P. Carniti, A. Gervasini, Calorimetry and Thermal Methods in Catalysis, in: A. Auroux (Ed.), Calorim. Therm. Methods Catal., Springer-V, Springer Berlin Heidelberg, Berlin, Heidelberg, 2013: pp. 543–551. doi:10.1007/978-3-642-11954-5.

[23] P. Carniti, A. Gervasini, S. Biella, Determination of Catalyst Surface Acidity in Liquids by a Pulse Liquid Chromatographic Technique, Adsorpt. Sci. Technol. 23 (2005) 739–749.

[24] T. Deblonde, C. Cossu-Leguille, P. Hartemann, Emerging pollutants in wastewater: A review of the literature, Int. J. Hyg. Environ. Health. 214 (2011) 442–448. doi:10.1016/j.ijheh.2011.08.002.

[25] D.J. Lapworth, N. Baran, M.E. Stuart, R.S. Ward, Emerging organic contaminants in groundwater: A review of sources, fate and occurrence, Environ. Pollut. 163 (2012) 287–303. doi:10.1016/j.envpol.2011.12.034.

[26] F. Mazille, T. Schoettl, N. Klamerth, S. Malato, C. Pulgarin, Field solar degradation of pesticides and emerging water contaminants mediated by polymer films containing titanium and iron oxide with synergistic heterogeneous photocatalytic activity at neutral pH, Water Res. 44 (2010) 3029–3038. doi:10.1016/j.watres.2010.02.026.

[27] M.A. Behnajady, H. Eskandarloo, N. Modirshahla, M. Shokri, Sol-gel low-temperature synthesis of stable anatase-type TiO_2 nanoparticles under different conditions and its photocatalytic activity, Photochem. Photobiol. 87 (2011) 1002–1008. doi:10.1111/j.1751-1097.2011.00954.x.

[28] B. Lin, C. Xue, X. Yan, G. Yang, G. Yang, B. Yang, Facile fabrication of novel SiO_2/g-C_3N_4 core–shell nanosphere photocatalysts with enhanced visible light activity, Appl. Surf. Sci. 357 (2015) 346–355. doi:10.1016/j.apsusc.2015.09.041.

[29] B. Lin, G. Yang, B. Yang, Y. Zhao, Construction of novel three dimensionally ordered macroporous carbon nitride for highly efficient photocatalytic activity, Appl. Catal. B Environ. 198 (2016) 276–285. doi:10.1016/j.apcatb.2016.05.069.

[30] I. Dalmázio, T.M.A. Alves, R. Augusti, An appraisal on the degradation of paracetamol by TiO_2/UV system in aqueous medium: product identification by gas chromatography-mass spectrometry (GC-MS), J. Braz. Chem. Soc. 19 (2008) 81–88. doi:10.1590/S0103-50532008000100013.

[31] E. Moctezuma, E. Leyva, C.A. Aguilar, R.A. Luna, C. Montalvo, Photocatalytic degradation of paracetamol: Intermediates and total reaction mechanism, J. Hazard. Mater. 243 (2012) 130–138. doi:10.1016/j.jhazmat.2012.10.010.

[32] L. Yang, L.E. Yu, M.B. Ray, Degradation of paracetamol in aqueous solutions by TiO_2 photocatalysis, Water Res. 42 (2008) 3480–3488. doi:10.1016/j.watres.2008.04.023.

[33] R. Andreozzi, V. Caprio, R. Marotta, D. Vogna, Paracetamol oxidation from aqueous solutions by means of ozonation and H_2O_2/UV system, Water Res. 37 (2003) 993–1004.

[34] D. Vogna, R. Marotta, A. Napolitano, M. D'Ischia, Advanced Oxidation Chemistry of Paracetamol. UV/H_2O_2-Induced Hydroxylation/Degradation Pathways and ^{15}N-Aided Inventory of Nitrogenous Breakdown Products., J. Org. Chem. 67 (2002) 6143–6151. doi:10.1021/jo025604v.

[35] L. Yang, L.E. Yu, M.B. Ray, Photocatalytic Oxidation of Paracetamol: Dominant Reactants, Intermediates, and Reaction Mechanisms, Environ. Sci. Technol. 43 (2009) 460–465. doi:10.1021/es8020099.

[36] O.-O. Prieto-Mahaney, N. Murakami, R. Abe, B. Ohtani, Correlation between Photocatalytic Activities and Structural and Physical Properties of Titanium(IV) Oxide Powders, Chem. Lett. 38 (2009) 238–239. doi:10.1246/cl.2009.238.

[37] D.C. Hurum, A.G. Agrios, K.A. Gray, T. Rajh, M.C. Thurnauer, Explaining the Enhanced Photocatalytic Activity of Degussa P25 Mixed-Phase TiO_2 Using EPR, J. Phys. Chem. B. 107 (2003) 4545–4549. doi:10.1021/jp0273934.

[38] H.G. Yang, C.H. Sun, S.Z. Qiao, J. Zou, G. Liu, S.C. Smith, et al., Anatase TiO_2 single crystals with a large percentage of reactive facets, Nature. 453 (2008) 638–641. doi:10.1038/nature06964.